Cellular and molecular changes to cortical neurons following low intensity repetitive magnetic stimulation at different frequencies

Stephanie Grehl (1,4), Helena Viola (2), Paula I Fuller-Carter (1), Kim W Carter (3), Sarah A Dunlop (1), Livia Hool (2), Rachel M Sherrard*(2,4), Jennifer Rodger* (1)

School of Animal Biology (1) and Anatomy, Physiology and Human Biology (2) , Telethon Institute for Child Health Research, Centre for Child Health Research, University of Western Australia, Perth, Australia (3) and Sorbonne Universités, UPMC Univ Paris 06 & CNRS, IBPS-B2A UMR 8256 Biological Adaptation and Ageing, Paris France (4).

* These two are co-senior authors

Corresponding author:

A/Prof Jennifer Rodger

Experimental and Regenerative Neurosciences M317

School of Animal Biology

University of Western Australia

35 Stirling Highway

Crawley WA 6009

Tel: (+618) 6488 2245

email: jennifer.rodger@uwa.edu.au

ABSTRACT

Repetitive transcranial magnetic stimulation (rTMS) is increasingly used as a treatment for neurological dysfunction and therapeutic effects have also been reported for low intensity rTMS (LI-rTMS) although these remain poorly understood. Our study describes for the first time a systematic comparison of the cellular and molecular changes in neurons *in vitro* induced by low intensity magnetic stimulation at different frequencies. We applied 5 different low intensity repetitive magnetic stimulation (LI-rMS) protocols to neuron-enriched primary cortical cultures for 4 days and assessed survival, and morphological and biochemical change. We show pattern-specific effects of LI-rMS: simple frequency pulse trains (10 Hz and 100 Hz) impaired cell survival, while more complex stimulation patterns (theta-burst and a biomimetic frequency) did not. Moreover, only 1 Hz stimulation modified neuronal morphology, inhibiting neurite outgrowth. To understand mechanisms underlying these differential effects, we measured intracellular calcium concentration during LI-rMS and subsequent changes in gene expression. All LI-rMS frequencies increased intracellular calcium, but rather than influx from the extracellular milieu typical of depolarisation, all frequencies induced calcium release from neuronal intracellular stores. Furthermore, we observed pattern-specific changes in expression of genes related to apoptosis and neurite outgrowth, which were consistent with our morphological data on cell survival and neurite branching. Thus, in addition to the known effects on cortical excitability and synaptic plasticity, our data demonstrate that LI-rMS can change the survival and structural complexity of neurons. These findings provide a cellular and molecular framework for understanding what low intensity magnetic stimulation may contribute to human rTMS outcomes.

Key index words or phrases: pulsed magnetic fields, repetitive transcranial magnetic stimulation, rTMS, cortical neurons, calcium signalling

Introduction

Repetitive transcranial magnetic stimulation (rTMS) is used in clinical treatment to non-invasively stimulate the brain and promote long-term plastic change in neural circuit function [1, 2], with benefits for a wide range of neurological disorders [3-5]. In addition, there is increasing evidence that low intensity magnetic stimulation (LI-rTMS) may also be therapeutic, particularly in mood regulation and analgesia [6-8]. Nonetheless, clinical outcomes of rTMS and LI-rTMS are variable [9] and greater knowledge of the mechanisms underlying different stimulation regimens is needed in order to optimise these treatments.

Investigating the mechanisms of both high and low intensity rTMS is important because most human rTMS protocols deliver a range of stimulation intensities across and within the brain. Human rTMS is most commonly delivered using butterfly figure-of-eight shaped coils [10, 11] to produce focal high-intensity fields that depolarise neurons in a small region of the cortex underlying the intersection of the 2 loops [10, 11], which in turn can modulate activity in down-stream neural centres [12, 13]. However, this stimulation focus is surrounded by a weaker magnetic field such that a large volume of adjacent cortical and sub-cortical tissue is also stimulated, albeit at a lower intensity that is below activation threshold [14, 15]. While the functional importance of this para-focal low-intensity stimulation in the context of human rTMS is unclear, low-intensity magnetic stimulation on its own modifies cortical function [16, 17] and brain oscillations [18]. Moreover, animal and *in vitro* studies demonstrate that low-intensity stimulation alters calcium signalling [19, 20], gene expression [21], neuroprotection [22] and the structure and function of neural circuits [23, 24]. However, the mechanisms underlying outcomes of low-intensity magnetic stimulation, particularly in conjunction with different stimulation frequencies, have not been investigated.

To address this, we undertook a systematic investigation of the fundamental morphological and molecular effects of five repetitive low intensity magnetic stimulation (LI-rMS) protocols in a simple *in vitro* system with defined magnetic field parameters. We show for the first time that LI-rMS induces calcium release from intracellular stores. Moreover, we show specific effects of different stimulation protocols on neuronal survival and morphology and associated changes in expression of genes mediating apoptosis and neurite outgrowth. Taken together, our data demonstrate that even low intensity magnetic stimulation induces long-term modifications to neuronal structure, which might have implications for understanding the effects of high-intensity human rTMS in the whole brain.

METHODS

Animals

C57Bl/6j mice pups were sourced from the Animal Resources Centre (Canning Vale, WA, Australia). Experimental procedures were approved by the UWA Animal Ethics Committee (03/100/957).

Tissue culture

To investigate changes in neuron biology following LI-rMS stimulation, we used neuronal enriched cultures from postnatal day 1 mouse cortex. Pups were euthanased by pentobarbitone sodium (150 mg/kg i.p.), decapitated and both cortices removed. Pooled cortical tissue was dissociated and prepared following standard procedures [25]. Cells were suspended in NB media (Neurobasal-A, 2 % B27 (Gibco®), 0.6 mg/ml creatine, 0.5 mM L-glutamine, 1 % Penicillin/Streptomycin, and 5 mM Hepes) and plated on round poly-D-lysine coated coverslips at a density of 75000 cells/well (day 0 *in vitro*; DIV 0). On DIV 3, half the culture medium was removed and replaced with fresh media containing cytosine arabinofuranoside (6 μM; Sigma) to inhibit glial proliferation. Cells were grown at 37°C in an incubator (5% CO_2 + 95% air) for 10 days and half the medium was replaced on DIV 6 and 9. To ensure that any experimental effects were not due to either different litters or culture sessions, plated coverslips from each litter were randomly allocated to stimulation groups. The whole culture-stimulation procedure was repeated 3 times.

Repetitive Magnetic Stimulation

LI-rMS stimulation was delivered to cells in the incubator with a custom built round coil (8 mm inside diameter, 16.2 mm outside diameter, 10 mm thickness, 0.25 mm copper wire, 6.1 Ω resistance, 462 turns) placed 3 mm from the coverslip (Fig 1A) and driven by a 12 V magnetic pulse generator: a simple resistor-inductor circuit under control of a programmable (C-based code) micro-controller card (CardLogix, USA). The non-sinusoidal monophasic pulse [26] had a measured 320μs rise time and generated an intensity of 13 mT as measured at the target cells by hall effect (ss94a2d, Honeywell, USA) and assessed by computational modelling using Matlab (Mathworks, USA; Fig 1B,C). Coil temperature did not rise above 37^{o}C, ruling out confounding effects of temperature change. Vibration from the bench surface (background) and the top surface of the coil were measured at 10 Hz stimulation using a single-point-vibrometer (Polytec, USA); coil vibration was within vibration amplitude of background (Fig 1D).

Stimulation was delivered for 10 continuous minutes per day at 1 of 5 frequencies: 1 Hz, which reduces, or 10 Hz which increases, cortical excitability in human rTMS [27, 28]; we also used 100 Hz, consistent with very low intensity pulsed magnetic field stimulation [29, 30], continuous theta burst stimulation (cTBS: 3 pulses at 50 Hz repeated at 5 Hz) showing inhibitory effects on cortical excitability post-stimulation in human rTMS [31, 32] or biomimetic high frequency stimulation (BHFS: 62.6 ms trains of 20 pulses, repeated at 9.75 Hz). The BHFS pattern was designed on electro-biomimetic principles [33], based on the main parameter from our previous studies [23, 24]} which was modelled on endogenous patterns of electrical fields around activated nerves during exercise (patent PCT/AU2007/000454, Global Energy Medicine). The total number of pulses delivered for each stimulation paradigm is shown in Table 1. We chose a standard duration of stimulation

of 10 minutes (rather than a standard number of pulses) because studies of brain plasticity reveal that 10 minutes of physical training or LI-rTMS is sufficient to induce functional and structural plasticity [23, 24, 34]. For all experiments, controls were treated identically but the coils were not activated. An overview of experiments and summary of experimental design is shown in Fig 1E.

Immunohistochemistry

To investigate the influence of different stimulation frequencies at the cellular level, we used immunohistochemistry to examine neuronal survival and the prevalence of different cell types. Cells plated on glass coverslips were grown in 12 spatially separated wells of a 24 well plate to ensure no overlap of magnetic field. Wells were stimulated for 10 minutes daily from DIV 6-9 and cells were fixed with 4% paraformaldehyde 24 hours after the last stimulation. Mouse anti-active Caspase-3 (1:50, Abcam) and TUNEL (DeadEnd™ Fluorometric TUNEL System, Promega) double labelling were carried out to identify apoptosis. Glia and neurons were labelled with rabbit anti-GFAP (1:500, Dako) or mouse anti-βIII Tubulin (1:500, Covance). Subpopulations of neurons were identified, using rabbit anti-calbindin D-28K (inhibitory and small excitatory neurons; 1:500, Chemicon [35]) or mouse anti-SMI-32 (excitatory neurons; 1:2000, Covance [36]). Antibody binding was visualised using fluorescently labelled secondary antibodies (Alexa Fluor 546 and Alexa Fluor 488; Invitrogen). Cell nuclei were labelled with either Hoechst (1:1000, Sigma Aldrich) or Dapi (DeadEnd™). Coverslips were mounted with Fluoromount-G.

Histological Analysis

For each experimental group, histological analyses were performed blind to stimulation paradigm on 12-18 images containing cultured cells from 2-3 different litters. Five semi-randomly distributed images per immunostained coverslip were taken from locations underneath the desired magnetic field (13 mT), in order to analyse cells that had received similar stimulation intensity. We counted cells labelled with the following antibody combinations: βIII Tubulin or GFAP (neurons/glia), Caspase-3 and TUNEL (apoptotic cells), or Calbindin or SMI-32 (inhibitory/excitatory neurons). Raw counts were normalized to the total cells numbers (Hoechst or DAPI labelled) in the analysed field (FA). Cells that were not immunolabelled for either marker were identified as 'other' and included in the total cell count.

Morphometric analysis was undertaken on individually visualized neurons. Calbindin labelled neurons had weakly labelled processes thus neurite morphology could not be reliably distinguished. Thus, only SMI-32 positive cells were analysed. For every cell, the longest neurite was traced and its total length calculated with Image J. To estimate neuronal morphology, fast Sholl analysis [37] was performed, using an Image-Pro®Plus (Media Cybernetics, Inc.) based macro (M. Doulazmi, UPMC).

Calcium Imaging

To assess the mechanisms underlying LI-rMS effects, we measured real-time changes in intracellular calcium during stimulation. On DIV 6-10, cells were incubated in 1 µM Fura-2AM (Molecular Probes) supplemented media at 37°C for 90-120 min. Immediately prior to experimentation, cells were transferred to Fura-2AM supplemented imaging solution containing: 140 mM NaCl, 5 mM KCl, 2.5 mM $CaCl_2$, 0.5 mM $MgCl_2$, 10 mM Glucose and

10 mM Hepes (pH 7.4). Intracellular calcium was assessed at 37°C as described previously [38] to evaluate ratiometric change and estimate intracellular concentration $[Ca^{2+}]_i$ (nM). Fura-2 340/380 nm ratiometric fluorescence was captured using a Hamamatsu Orca ER digital camera attached to an inverted Nikon TE2000-U microscope (ex 340/380 nm, em 510 nm) and analysed by manually tracing cells in MetaMorph® 6.3 (Molecular Devices).

Ratiometric fluorescent values were recorded from 5 min pre-stimulation to 5 min post-stimulation (or control) at 1 minute time intervals. Analyses were made off-line such that the experimenter was blind to stimulation group. Ratiometric fluorescent values were averaged over the last 3 min of stimulation ($\mu_{Main:}$ minutes 8-10), and normalised to the pre-stimulation baseline (μ_{Pre}: minutes 3-5). Percentage Fura-2 ratiometric signal change ($Y_{\%change}$) was calculated ($Y_{\%change} = ((\mu_{Pre} - \mu_{Main})/ \mu_{Main}) * 100$) (Fig 1E). Pilot experiments showed that there was no effect of culture age (DIV) on calcium responses, thus data were pooled across days.

Following each experiment, cells were fixed with 4% paraformaldehyde and immunostained for GFAP/βIII Tubulin/Hoechst, as described above, to confirm that imaged cells were neurons. Only data from βIII tubulin-positive neurons were included in the analysis.

To investigate the source of increased intracellular calcium, we assessed alterations in intracellular calcium when neurons were either placed in calcium-free imaging solution, or exposed to thapsigargin (3 μM, SIGMA) to deplete intracellular calcium stores. For calcium-free studies, cells were placed in calcium-free imaging solution (140 mM NaCl, 5 mM KCl, 0.5 mM $MgCl_2$, 10 mM HEPES, 10 mM Glucose, 3 mM EGTA, pH 7.4) immediately prior to experimentation. To confirm that results were not based on changes in ion concentration, in some experiments we compensated for the drop in Ca^{2+} with an equi-molar replacement of Mg^{2+} to keep a constant surface charge effect across the membrane. Results showed no

difference between these 2 solutions. Thapsigargin studies (supplemented 10 min prior to experimentation) were performed in normal 2.5 mM calcium containing imaging solution. All imaging solutions were supplemented with 1 µM Fura-2AM. Cell viability was confirmed with propidium iodide (PI) post-stimulation and cells that were permeable to PI were excluded from subsequent analysis.

PCR Array

To investigate the molecular events triggered by different frequency stimulation, changes in gene expression were examined in a separate series of cultures following a single stimulation at DIV 6. For each group (3 frequencies plus control), three replicates of ten wells underwent one stimulation session. Five hours after the end of stimulation, total RNA was extracted with Trizol (Life Technologies) followed by purification on RNeasy kit columns (Qiagen). cDNA was transcribed from 200 ng of total RNA using the RT² Easy First Strand cDNA Synthesis Kit (Qiagen). For each sample, 250 ng of cDNA was applied to the Mouse cAMP / Ca^{2+} Signaling Pathway Finder PCR Array and amplified on a Rotorgene 6000. Results were analysed by a researcher (K Carter), who did not know the tissue groupings, on the Qiagen RT^2 Profiler PCR array data analysis (v3.5) using the geometric mean of housekeeping genes glyceraldehyde-3-phosphate dehydrogenase and glucuronidase beta. Normalized mean expression levels (log2(2-ΔCt)) were used to determine differentially expressed genes between each group and control. Changes in gene expression were analysed further in R 3.0.1 using the NMF package [39], Ingenuity Pathways Analysis (IPA) and WebGestalt [40].

Statistical analysis

Data from all groups were explored for outliers and normal distribution with SPSS Statistics 20 (IBM). For cell survival and calcium imaging experiments, effects of frequency were analysed with One-way Analysis of Variance (Kruskal-Wallis; H) and Mann-Whitney (U) pairwise comparisons with Bonferroni-Dunn correction where appropriate. Neurite length data was analysed with Univariate ANOVA (F). Gene expression levels from the PCR array were compared by two sample *t*-test. All values are expressed as mean ± SEM and considered significant at $p < 0.05$.

RESULTS

We delivered multiple sessions of LI-rMS (DIV6-9) to see the cumulative effects on the survival and morphology of single neurons. We then examined potential mechanisms underpinning these cellular effects by identifying acute changes induced by a single session of LI-rMS: (1) intracellular calcium during stimulation; (2) gene expression 5hrs after a single stimulation session, an interval necessary for transcriptional changes to have occurred. The experimental design is summarized in Fig 1E.

rMS stimulation-specific effects on neuronal survival and morphology

We first investigated whether low intensity LI-rMS had deleterious effects and induced apoptosis by counting cells double labeled for Caspase-3 and TUNEL ($N_{\text{fields analyzed (FA)}}$: Control = 22; 1 Hz = 10; 10 Hz = 10; 100 Hz = 9; cTBS = 10; BHFS = 10). While the great majority of cells (about 90%) continued growing normally, there was a small but significant increase of apoptotic cells in cultures stimulated at 10 Hz (11.11 % ± 1.84) and 100 Hz (11.08 % ± 1.79) compared to unstimulated controls (4.3 % ± 0.9; p = 0.036 and 0.044 respectively, Fig 2A). In contrast, stimulation by 1 Hz and complex frequencies did not significantly alter apoptosis (~ 4-7% cells in each group). Because stimulation at 100 Hz did not induce more apoptosis than 10 Hz, it was not investigated further.

We next evaluated whether different LI-rMS patterns altered the proportions of neurons and glia in primary cortical cultures (N_{FA}: Control = 19; 1 Hz = 18; 10 Hz = 18; cTBS = 18; BHFS = 15). The ratio of neurons-to-glia following stimulation at any frequency was no different from unstimulated control cultures (Fig 2B,C), suggesting that the small amount of

apoptosis (~ 4-7%) involved all cell types equally. On average, pooled across all frequencies, we observed 85.6 % ± 1.1 neurons, 5.1 % ± 1.3 glia and 9.3 % undefined cells in our cultures. Because some studies have shown that magnetic fields differentially affect inhibitory and excitatory neurons [41, 42] we quantified the proportions of two neuronal populations: calbindin D-28K-positive neurons, which are predominantly inhibitory [35], and SMI-32-labelled excitatory neurons (N_{FA}: Control = 24; 1 Hz = 13; 10 Hz = 25; cTBS = 16; BHFS = 14). The higher proportion of inhibitory neurons in early postnatal cultures is in line with previous studies [43]. Only 1 Hz stimulation altered the relative proportions by increasing that of calbindin positive neurons ($p = 0.001$), from 81.6 % ± 1.8 in control cultures to 92.2 % ± 1.7, while decreasing the percentage of SMI-32 positive neurons ($p = 0.029$), from 4.1 % ± 0.8 in control cells to 0.8 % ± 0.3 (Fig. 2D,E). This reduction in number of SMI-32 positive cells (3.3 %) is within the 4-7% cell death observed in control and 1 Hz stimulated cultures (Fig 2A) and suggests that LI-rMS at 1 Hz slightly impaired survival of SMI-32 positive excitatory neurons without increasing apoptosis overall.

We then investigated neurite branching and outgrowth from individual SMI-32 positive neurons (N: Control = 24; 1 Hz = 8; 10 Hz = 14; cTBS = 7; BHFS = 11). Stimulation at 1 Hz significantly reduced neurite branching and outgrowth by 60% compared to control neurons (Fig 3A-E; $p = 0.001$). Sholl analysis revealed that changes occurred 10-50 µm from the soma (Fig 3E). However, the length of the longest neurite of each SMI-32 positive neuron was not significantly different between stimulation frequencies ($F = 0.936$, $p = 0.45$).

LI-rMS releases calcium from intracellular stores

To identify mechanisms that may explain these morphological and cell survival data, we examined changes in intracellular calcium during stimulation. Compared to unstimulated controls, each of 10 Hz, cTBS and BHFS stimulation significantly increased Fura-2 ratiometric fluorescence ($p < 0.001$; Fig 4A) by 11–13 % (Control: 2.1 % ± 0.8; 10 Hz: 13.4 % ± 2.3; cTBS: 15.0 % ± 2.6 and BHFS: 15.1 % ± 2.0). This is equivalent to an average change in intracellular Ca^{2+} from 34.31 nM ± 7.44 in control to 414.77 nM ± 41.52 after 10 min stimulation, a rise which is in the range of increased Ca^{2+} concentration following action potential induction [44, 45]. In contrast, 1 Hz stimulation induced an intermediate increase (8.3 % ± 1.1) in Fura-2 ratiometric fluorescence which was not significantly different from either unstimulated control or other stimulation frequencies (Fig 4A). No impact on neuronal viability was observed following a single session of LI-rMS stimulation (data not shown).

To determine whether the increase in intracellular calcium originated from the extracellular milieu or intracellular stores, we stimulated neurons either in calcium-free imaging solution, or after thapsigargin treatment (Fig 4B). Because of apparent equivalence of effect for cTBS and BHFS stimulation in previous experiments, pharmacological tests were carried out on 1 Hz, 10 Hz and BHFS frequencies. For all frequencies, the increase in neuronal Fura-2 ratiometric fluorescence under calcium-free conditions was not significantly different from that in normal imaging media (1 Hz: 10.7 % ± 2.5; 10 Hz: 14.7 % ± 1.8 and BHFS: 14.7 % ± 1.7). In contrast, exposure of cells to thapsigargin resulted in strong attenuation of the Fura-2 signal during stimulation at all frequencies ($p < 0.05$; 1 Hz: 1.5 % ± 1.4, 10 Hz: 4.6 % ± 2.4 and BHFS: 0.4 % ± 0.4). These data indicate that LI-rMS stimulation induces release of Ca^{2+} from intracellular stores rather than influx from the extracellular milieu (Fig 4B).

LI-rMS changes expression of genes implicated in neuronal survival

To further understand how LI-rMS may lead to changes in cell survival and morphology, we examined the immediate up-and down-regulation of genes associated with Ca^{2+} signaling, five hours after a single session of stimulation at different frequencies. We identified 16 genes (Table 2; Fig 5A) for which expression changes were significantly different from unstimulated controls ($p < 0.05$) in at least one of the three experimental groups (Fig 5B). Enrichment analysis on these 16 genes in IPA and gene ontology terms (Webgestalt; supplementary Table 1) revealed that 15 of the 16 genes were significantly associated with two major biofunctions: 1) cell survival and apoptosis and 2) cell morphology and migration (Fig 5C). The remaining gene, slc18a1 encodes a vesicular monoamine transporter and was significantly increased following stimulation with 10 Hz.

All LI-rMS frequencies induced changes in genes situated within neuronal survival or apoptosis pathways (Fig 6A,B), of which some were common to all frequencies (ENO2 and CRH), and others pattern-specific (Figs 5B, 6A,B; Table 2). 10 Hz stimulation, which was associated with apoptosis, upregulated pro-apoptotic genes (e.g. Pmaip1/Noxa, and BRCA1) and downregulated anti-apoptotic genes (e.g. JunD). In addition, stimulation by frequencies which did not induce apoptosis resulted in pro-survival changes to gene expression (eg. 1 Hz upregulated hexokinase and BHFS downregulated cdk5 and Sod2). These data also show that although all our LI-rMS paradigms altered intracellular Ca^{2+}, the downstream effects on gene expression were specific for each stimulation frequency and rhythm.

DISCUSSION

This study used cortical neuron cultures to identify cellular and molecular mechanisms underlying the outcomes of different low intensity magnetic stimulation parameters. Our data show differential effects of specific LI-rMS paradigms on neuronal survival and morphology. Furthermore, evidence for calcium release from intracellular stores and stimulation-specific regulation of gene expression identify a potential cellular and molecular framework for understanding what low intensity magnetic stimulation may contribute to rTMS outcomes in humans.

Paradigm-specific effects on neuronal survival: dose vs rhythm

Our study shows specific effects of different LI-rMS paradigms on neuronal survival, suggesting that the overall stimulation load (pulse number and density) and/or rhythm of pulse delivery may be important. It has recently been proposed that there is no simple dose-dependent cumulative effect of rTMS on the cerebral cortex [46]. Our data on isolated cortical neurons, showing that several low-intensity stimulation paradigms induce similar changes to intracellular calcium concentration but different patterns of gene expression and cell survival, extend this hypothesis to suggest that pulse rhythm, i.e. the pattern of stimulation frequency, is a primary determinant.

Considering pulse trains delivered at simple frequencies, increasing stimulation load (pulses/unit time) is associated with an increase in intracellular Ca^{2+} and cell death. In the group that received the lowest number of pulses (1 Hz: 600 pulses), there was only an intermediate non-significant increase in intracellular Ca^{2+} and a level of apoptosis that was within the range observed in control cultures (4%). Moreover, increasing stimulation load

with 10 and 100 Hz (6000 and 60,000 pulses within the 10 min stimulation period), significantly increased intracellular Ca^{2+} and overall cellular apoptosis, consistent with the deleterious effect of prolonged magnetic stimulation to human monocyte leukemia cells [47]. Such fundamental biological knowledge will be important to future human rTMS as advances in coil cooling will permit longer stimulation trains without frequent TMS-free pauses seen in current clinical practice [5]. In contrast, even higher stimulation load, but delivered with a complex biomimetic frequency (TBS: 7000 and BHFS: 120000 pulses within 10 minutes) did not increase neuronal apoptosis despite rises in intracellular Ca^{2+} similar to those following 10 Hz. This not only confirms the hypothesis that dose and effect are not simply related [46, 48], but suggests that the rhythm with which the pulses are delivered is fundamental to their effect. By mimicking endogenous patterns of neuronal firing, biomimetic complex waveforms may induce more intricate and biologically safe changes compared to simple frequencies [28, 33]. One possible mechanism underlying these observations is frequency- and pattern-specific regulation of calcium buffering proteins [49-51], which is likely to contribute to the complex relationship between stimulation load, regulation of intracellular Ca^{2+} levels and cell viability. Indeed the promising therapeutic outcomes in human patients using TBS, albeit at high intensity [52, 53], would appear to support the hypothesis. Thus our data shows a complex interplay between pulse frequency, rhythm and outcome, confirms the recent suggestion that appropriately designed rTMS protocols may generate highly adaptable therapies to treat a wide range of neurological conditions [5].

The possibility that the effect of LI-rMS is determined by the number and/or rhythm of pulses was supported by our gene expression studies, which show that 1 Hz results in fewer gene-expression changes than 10 Hz and BHFS stimulation and BHFS alters a greater number of genes than 10 Hz. The majority of the regulated genes in our study were associated with cell survival and apoptosis pathways (Fig 5C), consistent with evidence for pro-survival [22] or

pro-apoptotic [47, 54] effects of magnetic fields and our survival data (discussed above). All frequencies in our study downregulated neuron-specific enolase (ENO2) and corticotrophin-releasing hormone (CRH), both of which have neuroprotective properties [55, 56]. However, in addition, we show paradigm-specific regulation of genes within neuronal survival and apoptosis pathways. Increased apoptosis after 10 Hz stimulation was associated with the upregulation of pro-apoptotic [57, 58] and downregulation of anti-apoptotic genes [59, 60]. In contrast, stimulation by frequencies which did not induce apoptosis showed survival-promoting gene expression changes [61, 62]. Given that neuroprotective effects of rTMS remain controversial [63], further characterisation of these gene expression changes at the protein and functional level could identify novel neuroprotective therapies for treatment of neurological disorders.

Stimulation-specific effects of LI-rMS on neuronal morphology: implications for reorganisation of cortical circuits

In addition to effects on neuronal survival, our data also shows a stimulation pattern-specific effect on neuronal morphology. 1 Hz stimulation reduced neurite complexity of glutamatergic projection neurons, consistent with a recent study in hippocampal neurons *in vitro* demonstrating that 1 Hz magnetic stimulation reduced dendritic branching and damaged synaptic structure [64]. This suggests that the intermediate rise in Ca^{2+} following 1 Hz stimulation, although statistically non-significant, has biological relevance. In addition, 1 Hz-induced neurite regression would have the net effect of reducing excitatory connectivity within a cortical circuit, which is consistent with the LTD-like effects of 1 Hz rTMS on the human cortex [65]. However, we studied dissociated neurons, with minimal contact between

neurites, suggesting that magnetic stimulation may directly alter neuronal structure beyond those changes (e.g. spines) associated with modulation from synaptic signalling [51, 66, 67].

Although we did not observe morphological changes when applying other frequencies, BHFS upregulated Cyr61, which is involved in the control of dendritic growth and has been associated with reorganisation of neuronal projections [68] and in association with longer treatment may contribute to the reorganization of abnormal circuitry induced by LI-rTMS at BHFS frequency [23, 24].

Intracellular Ca^{2+} increase: mechanism of cortical plasticity?

Changes in intracellular Ca^{2+} in response to magnetic fields have been demonstrated in a range of cells [19, 69, 70]. We show here for the first time that in neurons LI-rMS releases Ca^{2+} from intracellular stores. This provides a mechanism for LI-rMS induced cellular and molecular changes that is independent of action potential induction, given that the stimulation was subthreshold, estimated to be 0.5V/m [33], which is several orders of magnitude below the ~50V/m that depolarises neurons [46]. This concurs with our gene expression data in which markers of synaptic activity and action potential firing (e.g. CREB and BDNF) were not upregulated (data not shown). Importantly, calcium release from intracellular stores can modulate synaptic plasticity [71] even without action potential firing and associated calcium influx. Therefore our data provide a mechanism to explain the effects of low intensity magnetic stimulation on cortical neurons [17], and provides a cellular and molecular framework for understanding what low intensity magnetic stimulation may add to the altered calcium signalling induced by the high-intensity focus of human rTMS, and thus its potential contribution to human rTMS outcomes.

Elucidation of novel mechanisms: relevance of *in vitro* low intensity LI-rMS to human rTMS

As discussed above, we have identified changes to cell morphology, intracellular calcium flux and gene expression in isolated neurons stimulated by subthreshold low-intensity magnetic pulses. This experimental paradigm is *very different* from the peri-threshold high-intensity stimulation of whole neural networks in human rTMS; so what do our data contribute? First, our data reveal for the first time a fundamental cellular mechanism of non-depolarising magnetic fields on neurons, which in the *in vivo* context would underlie any trans-synaptic, neural circuit or cell environment responses. This could only be achieved by the application of a defined magnetic field to isolated cortical neurons, thus removing the confounding effects of glial responses and neuronal circuit activity from the observed outcomes. However, neurons that are maintained in culture are relatively immature, albeit fully differentiated, and not integrated within functioning neural networks. Thus their response to magnetic fields may be modified by different receptor and calcium-buffering capacities to adult neurons, especially in the absence of normal glial metabolic regulation and afferent activity. This, in turn, may make these neurons more susceptible to the low-intensity stimulation we induced in a manner that would not occur in the adult human brain even to higher intensity stimulation. Second, we identified potentially deleterious effects of 10 minutes continuous stimulation (slight increase in neuronal apoptosis) even at low intensity. Although such continuous pulse trains are not given in current human rTMS, the concern our data raise has pertinence to potential future human rTMS protocols as advances in coil-cooling technology may remove the requirement for short stimulation trains interspersed with TMS-free pauses. Taken together, our data demonstrate a novel cell-intrinsic mechanism for low intensity magnetic field stimulation of neurons which provides new insights into the structural and functional plastic changes described following low intensity magnetic stimulation [17, 23, 24, 30]. Importantly, this mechanism may also be evoked during high

intensity stimulation, thus potentially working together with previously described metabolic and synaptic plasticity mechanisms of human rTMS [64, 67, 72-74].

Conclusion

In summary, our data show that magnetic fields of different frequencies and rhythms alter intracellular calcium concentration and gene expression, which are consistent with long term modulation of neuronal survival. The immediate modification of calcium levels and gene expression support the development of long term changes following multiple stimulation sessions. Taken together with our previous study demonstrating that LI-rTMS can induce reorganization of neural circuits *in vivo* [23, 24] our data indicate that effects of low intensity stimulation as a by-product of high intensity rTMS coils cannot be disregarded. Although, our stimulation parameters did not directly mimic those used in human rTMS, the knowledge about mechanisms underlying the effects of different stimulation paradigms provided by this study will contribute to understanding magnetic stimulation outcomes and optimizing therapeutic application in humans.

Acknowledgements

Funded by an Australian Research Council (ARC) Linkage grant LP110100201, the National Health and Medical Research Council (NHMRC) Australia, the Neurotrauma Program (State Government of Western Australia, funded through the Road Trauma Trust Account, but the project does not reflect views or recommendations of the Road Safety Council) and a French CNRS PICS grant to support the international collaboration. SG is funded by UIS and SIRF grants, University of Western Australia. HV is funded by the National Heart Foundation.

KWC is supported by the McCusker Charitable Foundation Bioinformatics Centre. LH is an ARC Future Fellow and honorary NHMRC Senior research fellow, JR is a NHMRC Senior Research Fellow and SAD a NHMRC Principal Research Fellow.

We are grateful to Marissa Penrose and Michael Archer for technical assistance, Rob Woodward and Andrew Garrett for scientific advice and assistance and Mohamed Doulazmi for the fast Sholl Analysis program and scientific advice. Finally we would like to thank Global Energy Medicine Pty Ltd for the donation of stimulation devices.

REFERENCES

[1] Pell GS, Roth Y, Zangen A. Modulation of cortical excitability induced by repetitive transcranial magnetic stimulation: Influence of timing and geometrical parameters and underlying mechanisms. Prog Neurobiol. 2011;93(1):59-98.

[2] Thickbroom G. Transcranial magnetic stimulation and synaptic plasticity: experimental framework and human models. Exp Brain Res. 2007;180:583-93.

[3] Adeyemo BO, Simis M, Macea D, Fregni F. Systematic Review of Parameters of Stimulation: Clinical Trial Design Characteristics and Motor Outcomes in Noninvasive Brain Stimulation in Stroke. Front Psychiatr. [Review]. 2012;3(88).

[4] George MS, Taylor JJ, Short EB. The expanding evidence base for rTMS treatment of depression. Curr Op Psychiatr. 2013;26:13-8.

[5] Daskalakis ZJ. Theta-burst transcranial magnetic stimulation in depression: when less may be more. Brain. 2014;137:1860-2.

[6] Martiny K, Lunde M, Bech P. Transcranial low voltage pulsed electromagnetic fields in patients with treatment-resistant depression. Biol Psychiatr. 2010;68:163-9.

[7] Robertson JA, Theberge J, Weller J, Drost DJ, Prato FS, Thomas AW. Low-frequency pulsed electromagnetic field exposure can alter neuroprocessing in humans. J R Soc Interface. 2010 Mar 6;7:467-73.

[8] Di Lazzaro V, Capone F, Apollonio F, Borea PA, Cadossi R, Fassina L, et al. A consensus panel review of central nervous system effects of the exposure to low-intensity extremely low-frequency magnetic fields. Brain Stimul. 2013;6:469-76.

[9] Wassermann EM, Zimmermann T. Transcranial magnetic brain stimulation: Therapeutic promises and scientific gaps. Pharm Ther. 2012;133(1):98-107.

[10] Fatemi-Ardekani A. Transcranial Magnetic Stimulation: Physics, Electrophysiology, and Applications. Crit Rev Biomed Eng. 2008;36(5-6):375-412.

[11] Thielscher A, Kammer T. Electric field properties of two commercial figure-8 coils in TMS: calculation of focality and efficiency. Clin Neurophysiol. 2004;115(7):1697-708.

[12] Valero-Cabre A, Payne BR, Rushmore J, Lomber SG, Pascual-Leone A. Impact of repetitive transcranial magnetic stimulation of the parietal cortex on metabolic brain activity: a 14C-2DG tracing study in the cat. Exp Brain Res. 2005;163(1):1-12.

[13] Aydin-Abidin S, Trippe J, Funke K, Eysel UT, Benali A. High- and low-frequency repetitive transcranial magnetic stimulation differentially activates c-Fos and zif268 protein expression in the rat brain. Exp Brain Res. 2008;188(2):249-61.

[14] Cohen LG, Roth B, Nilsson J, Nguyet D, Panizza M, Bandinelli S, et al. Effects of coil design on delivery of focal magnetic stimulation. Technical considerations. Electroenceph Clin Neurophysiol. 1990;75:50-357.

[15] Deng Z-D, Lisanby SH, Peterchev AV. Electric field depth–focality tradeoff in transcranial magnetic stimulation: Simulation comparison of 50 coil designs. Brain Stim. 2013;6(1):1-13.

[16] Robertson JA, Théberge J, Weller J, Drost DJ, Prato FS, Thomas AW. Low-frequency pulsed electromagnetic field exposure can alter neuroprocessing in humans. J R Soc Interface. 2010;7(44):467-73.

[17] Capone F, Dileone M, Profice P, Pilato F, Musumeci G, Minicuci G, et al. Does exposure to extremely low frequency magnetic fields produce functional changes in human brain? J Neural Trans. 2009;116(3):257-65.

[18] Cook CM, Thomas AW, Prato FS. Resting EEG is affected by exposure to a pulsed ELF magnetic field. Bioelectromagnetics. 2004;25(3):196-203.

[19] Pessina GP, Aldinucci C, Palmi M, Sgaragli G, Benocci A, Meini A, et al. Pulsed electromagnetic fields affect the intracellular calcium concentrations in human astrocytoma cells. Bioelectromagnetics. 2001;22(7):503-10.
[20] Piacentini R, Ripoli C, Mezzogori D, Azzena GB, Grassi C. Extremely low-frequency electromagnetic fields promote in vitro neurogenesis via upregulation of Cav1-channel activity. J Cell Physiol. 2008;215(1):129-39.
[21] Mattsson M-O, Simkó M. Is there a relation between extremely low frequency magnetic field exposure, inflammation and neurodegenerative diseases? A review of in vivo and in vitro experimental evidence. Toxicology. 2012;301(1–3):1-12.
[22] Yang Y, Li L, Wang Y-G, Fei Z, Zhong J, Wei L-Z, et al. Acute neuroprotective effects of extremely low-frequency electromagnetic fields after traumatic brain injury in rats. Neurosci Letts. 2012;516(1):15-20.
[23] Rodger J, Mo C, Wilks T, Dunlop SA, Sherrard RM. Transcranial pulsed magnetic field stimulation facilitates reorganization of abnormal neural circuits and corrects behavioral deficits without disrupting normal connectivity. FASEB J. 2012;26(4):1593-606.
[24] Makowiecki K, Harvey A, Sherrard RM, Rodger J. Low-intensity repetitive transcranial magnetic stimulation improves abnormal visual cortical circuit topography and upregulates BDNF in mice. J Neurosci. 2014;34:10780 –92.
[25] Meloni BP, Majda BT, Knuckey NW. Establishment of neuronal in vitro models of ischemia in 96-well microtiter strip-plates that result in acute, progressive and delayed neuronal death. Neuroscience. 2001;108(1):17-26.
[26] Peterchev AV, Murphy DL, Lisanby SH. Repetitive transcranial magnetic stimulator with controllable pulse parameters. J Neural Eng. 2011;8(3):2922-6.
[27] Fitzgerald PB, Fountain S, Daskalakis ZJ. A comprehensive review of the effects of rTMS on motor cortical excitability and inhibition. Clin Neurophysiol. 2006;117:2584-96.
[28] Hoogendam JM, Ramakers GMJ, Di Lazzaro V. Physiology of repetitive transcranial magnetic stimulation of the human brain. Brain Stim. 2010;3(2):95-118.
[29] Ash M, Martin B, Edward E, Kuo-Chen C, Matthew S. G, Reba G. Steps to the clinic with ELF EMF. Natural Sci. 2009;1(3):157-65.
[30] Di Lazzaro V, Capone F, Apollonio F, Borea PA, Cadossi R, Fassina L, et al. A Consensus Panel Review of Central Nervous System Effects of the Exposure to Low-Intensity Extremely Low-Frequency Magnetic Fields. Brain Stim. 2013;6(4):469-76.
[31] Gamboa OL, Antal A, Laczo B, Moliadze V, Nitsche MA, Paulus W. Impact of repetitive theta burst stimulation on motor cortex excitability. Brain Stim. 2011;4:145-51.
[32] Huang Y-Z, Edwards MJ, Rounis E, Bhatia KP, Rothwell JC. Theta Burst Stimulation of the Human Motor Cortex. Neuron. 2005;45(2):201-6.
[33] Martiny K, Lunde M, Bech P. Transcranial Low Voltage Pulsed Electromagnetic Fields in Patients with Treatment-Resistant Depression. Biol Psychiatr. 2010;68:163-9.
[34] Angelov DN, Ceynowa M, Guntinas-Lichius O, Streppel M, Grosheva M, Kiryakova SI, et al. Mechanical stimulation of paralyzed vibrissal muscles following facial nerve injury in adult rat promotes full recovery of whisking. Neurobiol Dis. 2007;26:229-42.
[35] Brederode van JFM, Helliesen MK, Hendrickson AE. Distribution of the calcium-binding proteins parvalbumin and calbindin-D28k in the sensorimotor cortex of the rat. Neuroscience. 1991;44(1):157-71.
[36] DeFelipe J. Types of neurons, synaptic connections and chemical characteristics of cells immunoreactive for calbindin-D28K, parvalbumin and calretinin in the neocortex. J Chem Neuroanat. 1997;14(1):1-19.
[37] Gutierrez H, Davies AM. A fast and accurate procedure for deriving the Sholl profile in quantitative studies of neuronal morphology. J Neuroscience Meths. 2007;163(1):24-30.

[38] Viola HM, Arthur PG, Hool LC. Transient Exposure to Hydrogen Peroxide Causes an Increase in Mitochondria-Derived Superoxide As a Result of Sustained Alteration in L-Type Ca2+ Channel Function in the Absence of Apoptosis in Ventricular Myocytes. Circulation Res. 2007;100:1036-44.
[39] Gaujoux R, Seoighe C. A flexible R package for nonnegative matrix factorization. BMC Bioinform. 2010;11(1):367.
[40] Zhang B, Kirov S, Snoddy J. WebGestalt: an integrated system for exploring gene sets in various biological contexts. Nuc Acids Res. 2005;33(suppl 2):W741-W8.
[41] Benali A, Trippe J, Weiler E, Mix A, Petrasch-Parwez E, Girzalsky W, et al. Theta-Burst Transcranial Magnetic Stimulation Alters Cortical Inhibition. J Neurosci. 2011;31:1193-203.
[42] Meyer JF, Wolf B, Gross GW. Magnetic Stimulation and Depression of Mammalian Networks in Primary Neuronal Cell Cultures. IEEE Trans Biomed Eng. 2009;56:1512-23.
[43] Alho H, Ferrarese C, Vicini S, Vaccarino F. Subsets of GABAergic neurons in dissociated cell cultures of neonatal rat cerebral cortex show co-localization with specific modulator peptides. Brain Res. 1988 Apr 1;467(2):193-204.
[44] Liao CW, Lien CC. Estimating intracellular Ca2+ concentrations and buffering in a dendritic inhibitory hippocampal interneuron. Neuroscience. 2009;164(4):1701-11.
[45] Helmchen F, Borst JG, Sakmann B. Calcium dynamics associated with a single action potential in a CNS presynaptic terminal. Biophys J. 1997;72(3):1458-71.
[46] Volz LJ, Benali A, Mix A, Neubacher U, Funke K. Dose-Dependence of Changes in Cortical Protein Expression Induced with Repeated Transcranial Magnetic Theta-Burst Stimulation in the Rat. Brain Stim. 2013;6(4):598-606.
[47] Stratton D, Lange S, Inal JM. Pulsed extremely low-frequency magnetic fields stimulate microvesicle release from human monocytic leukaemia cells. Biochem Biophys Res Comm. 2013;430(2):470-5.
[48] Nettekoven C, Volz LJ, Kutscha M, Pool E-M, Rehme AK, Eickhoff SB, et al. Dose-Dependent Effects of Theta Burst rTMS on Cortical Excitability and Resting-State Connectivity of the Human Motor System. J Neurosci. 2014;34(20):6849-59.
[49] Gilabert JA. Cytoplasmic Calcium Buffering. In: Islam MS, editor. Calcium Signaling. London: Springer 2012.
[50] Chard PS, Bleakman D, Christakos S, Fullmer CS, Miller RJ. Calcium buffering properties of calbindin D28k and parvalbumin in rat sensory neurones. J Physiol. 1993;472(1):341-57.
[51] Funke K, Benali A. Modulation of cortical inhibition by rTMS – findings obtained from animal models. J Physiol. 2011;589(18):4423-35.
[52] Li C-T, Chen M-H, Juan C-H, Huang H-H, Chen L-F, Hsieh J-C, et al. Efficacy of prefrontal theta-burst stimulation in refractory depression: a randomized sham-controlled study. Brain. 2014;137(7):2088-98.
[53] Talelli P, Greenwood RJ, Rothwell JC. Exploring Theta Burst Stimulation as an intervention to improve motor recovery in chronic stroke. Clin Neurophysiol. 2007;118(2):333-42.
[54] Juszczak K, Kaszuba-Zwoinska J, Thor PJ. Pulsating electromagnetic field stimulation of urothelial cells induces apoptosis and diminishes necrosis: new insight to magnetic therapy in urology. J Physiol Pharmacol. 2012;63(4):397-401.
[55] Hattori T, Takei N, Mizuno Y, Kato K, Kohsaka S. Neurotrophic and neuroprotective effects of neuron-specific enolase on cultured neurons from embryonic rat brain. Neurosci Res. 1995;21(3):191-8.
[56] Lezoualc'h F, Engert S, Berning B, Behl C. Corticotropin-Releasing Hormone-Mediated Neuroprotection against Oxidative Stress Is Associated with the Increased Release of Non-

amyloidogenic Amyloid β Precursor Protein and with the Suppression of Nuclear Factor-κB. Mol Endocrinol. 2000;14(1):147-59.
[57] Seo Y-W, Shin JN, Ko KH, Cha JH, Park JY, Lee BR, et al. The Molecular Mechanism of Noxa-induced Mitochondrial Dysfunction in p53-Mediated Cell Death. J Biol Chem. 2003;278(48):48292-9.
[58] Thangaraju M, Kaufmann SH, Couch FJ. BRCA1 Facilitates Stress-induced Apoptosis in Breast and Ovarian Cancer Cell Lines. J Biol Chem. 2000;275(43):33487-96.
[59] Agarwal R, Agarwal P. Glaucomatous neurodegeneration: An eye on tumor necrosis factor-alpha. Indian J Ophthalmol. 2012;60:255-61.
[60] Weitzman JB, Fiette L, Matsuo K, Yaniv M. JunD Protects Cells from p53-Dependent Senescence and Apoptosis. Mol Cell. 2000;6(5):1109-19.
[61] Vincent AM, Russell JW, Sullivan KA, Backus C, Hayes JM, McLean LL, et al. SOD2 protects neurons from injury in cell culture and animal models of diabetic neuropathy. Exp Neurol. 2007;208(2):216-27.
[62] Zhang L, Liu W, Szumlinski KK, Lew J. p10, the N-terminal domain of p35, protects against CDK5/p25-induced neurotoxicity. Proc Natl Acad Sci. 2012;109(49):20041-6.
[63] Bates KA, Clark VW, Meloni BP, Dunlop SA, Rodger J. Short-term low intensity PMF does not improve functional or histological outcomes in a rat model of transient focal cerebral ischemia. Brain Res. 2012;1458(0):76-85.
[64] Ma J, Zhang Z, Su Y, Kang L, Geng D, Wang Y, et al. Magnetic stimulation modulates structural synaptic plasticity and regulates BDNF–TrkB signal pathway in cultured hippocampal neurons. Neurochem Int. 2013;62(1):84-91.
[65] Gerschlager W, Siebner HR, Rothwell JC. Decreased corticospinal excitability after subthreshold 1 Hz rTMS over lateral premotor cortex. Neurology. 2001;57(3):449-55.
[66] Majewska AK, Newton JR, Sur M. Remodeling of Synaptic Structure in Sensory Cortical Areas In Vivo. J Neurosci. 2006 March 15, 2006;26(11):3021-9.
[67] Vlachos A, Müller-Dahlhaus F, Rosskopp J, Lenz M, Ziemann U, Deller T. Repetitive Magnetic Stimulation Induces Functional and Structural Plasticity of Excitatory Postsynapses in Mouse Organotypic Hippocampal Slice Cultures. J Neurosci. 2012;32(48):17514-23.
[68] Malik AR, Urbanska M, Gozdz A, Swiech LJ, Nagalski A, Perycz M, et al. Cyr61, a Matricellular Protein, Is Needed for Dendritic Arborization of Hippocampal Neurons. J Biol Chem. 2013, 2013;288(12):8544-59.
[69] Huang J, Ye Z, Hu X, Lu L, Luo Z. Electrical stimulation induces calcium-dependent release of NGF from cultured Schwann cells. Glia. 2010;58(5):622-31.
[70] McCreary CR, Dixon SJ, Fraher LJ, Carson JJL, Prato FS. Real-time measurement of cytosolic free calcium concentration in Jurkat cells during ELF magnetic field exposure and evaluation of the role of cell cycle. Bioelectromagnetics. 2006;27(5):354-64.
[71] Hulme SR, Jones OD, Ireland DR, Abraham WC. Calcium-Dependent But Action Potential-Independent BCM-Like Metaplasticity in the Hippocampus. J Neurosci. 2012;32(20):6785-94.
[72] Gersner R, Kravetz E, Feil J, Pell G, Zangen A. Long-Term Effects of Repetitive Transcranial Magnetic Stimulation on Markers for Neuroplasticity: Differential Outcomes in Anesthetized and Awake Animals. J Neurosci. 2011;31(20):7521-6.
[73] Valero-Cabré A, Payne B, Rushmore J, Lomber S, Pascual-Leone A. Impact of repetitive transcranial magnetic stimulation of the parietal cortex on metabolic brain activity: a 14C-2DG tracing study in the cat. Exp Brain Res. 2005;163(1):1-12.
[74] Allen EA, Pasley BN, Duong T, Freeman RD. Transcranial Magnetic Stimulation Elicits Coupled Neural and Hemodynamic Consequences. Science. 2007;317(5846):1918-21.

Figure legends

Figure 1 Stimulation apparatus and experimental design: A: photographs of an *in vitro* stimulation coil used in this study. Views are from the top (top panel) and side (bottom panel). The diagram in the bottom panel shows that the coil was placed beneath one well of a 24 well culture dish containing a coverslip (blue) with culture medium (pink). The coil (orange) was located at a distance of 3 mm from the coverslip because of the thickness of the plastic base of the culture dish (white). Note that neighbouring wells did not contain coverslips to avoid interactions of magnetic fields from individual coils (compare extent of magnetic field and coverslip shown in C). B: Matlab software model representing the induced magnetic field at the level of the coil, distance in mm. C: Top view of modelled magnetic field strength at 3 mm from the base of the coil (position of the coverslip). Dashed circle represents the well and solid circle represents the edge of the cover slip (Ø = 13 mm). Black dots show the sampling locations for cell counts and morphological analysis**.** D: Fourier transform of the frequency spectrum of vibration measurement (mm/s) **taken by a single-point-vibrometer placed either on the bench surface (background) or on top of the coil (in place of the culture plate as illustrated in A)**. Vibration measured from background surface (black) and the coil (red) confirms that the coil did not generate vibration above background levels. E: Timeline for our experimental design. We delivered multiple sessions of LI-rMS (DIV6-9) to see the cumulative effects on the survival and morphology of single neurons. Then in separate experiments we examined potential mechanisms underpinning these cellular effects by identifying acute changes induced by a single session of LI-rMS: (1) intracellular calcium during stimulation; (2) gene expression 5 hrs after stimulation, an interval necessary for transcriptional changes to have occurred. The inset shows the detailed timeframe for intracellular calcium imaging, and is an example for DIV 6. LI-rMS was delivered for 10 minutes (grey zone). Ratiometric fluorescent values recorded over the last 3

min of stimulation were averaged and reported as a percentage of pre-stimulation baseline. Scale bar (A): 15 mm.

Figure 2: **LI-rMS alters cell survival**. A: Percentage cells double labeled for Caspase-3 and TUNEL were increased following 10 and 100 Hz compared to unstimulated controls ($H = 14.32$, $p = 0.014$. Pairwise comparisons Control-10 Hz: $U = -23.832$, $p = 0.036$ and Control-100 Hz: $U = -24.237$, $p = 0.044$). B,C: Percentage cells that were labeled with βIII Tubulin (neurons; B) or GFAP (glia; C) (Neuron: $H = 5.93$, $p = 0.204$, Glia: $H = 14.53$, $p = 0.006$. Pairwise comparisons (U): no significant difference to Control). D,E: Percentage cells that were labeled with Calbindin (D) or SMI-32 (E). 1 Hz increased the proportion of calbindin positive inhibitory neurons and decreased SMI-32 positive glutamatergic neurons compared to unstimulated controls ($H = 21.103$, $p = 0.000$. Pairwise comparisons Control-1 Hz: $U = -35.94$, $p = 0.001$. SMI-32: $H = 15.19$, $p = 0.004$. Pairwise comparisons Control-1 Hz: $U = 26.71$, $p = 0.029$). Error bars are standard error of the mean.

Figure 3: **LI-rMS has stimulation pattern-specific effects on neuronal morphology** A,B: Representative neuronal morphology from control (A) and 1 Hz (B) stimulation. C: diagram illustrating Sholl analysis. D: mean number of dendrite intersections per neuron following LI-rMS (4 days, 10 min per day) at different frequencies ($H = 17.84$, $p = 0.001$. Pairwise comparisons Control-1 Hz: $U = 30.771$, $p = 0.001$). E: Number of intersections per concentric Sholl circle from 10-80 µm from the soma are decreased in 1 Hz stimulated samples compared to unstimulated controls (10 µm: $U = 7.13$, $p = 0.008$, 20 µm: $U = 5.94$, $p = 0.015$, 30 µm: $U = 7.86$, $p = 0.005$, 40 µm: $U = 6.84$, $p = 0.009$, 50 µm: $U = 5.29$, $p = 0.021$). Error bars are standard error of the mean.

Figure 4: **LI-rMS induces Ca^{2+} release from intracellular stores.** Alterations in Fura-2 340/380 nm ratiometric fluorescence (% change Fura-2) in cortical neurons after a single 10 min stimulation with 1 Hz, 10 Hz, cTBS and BHFS frequencies. A: LI-rMS at each of 10 Hz, cTBS and BHFS increased intracellular calcium compared to unstimulated controls, while 1 Hz only generated an intermediate rise ($H = 20.7$, $p = 0.000$. Pairwise comparisons Control-10 Hz: $U= -27.97$, $p = 0.007$; Control-cTBS : $U = -32.48$, $p = 0.001$; Control-BHFS : $U = -38.03$, $p = 0.000$). B: LI-rMS induced similar increase in Fura-2 ratiometric fluorescence in normal imaging and calcium-free media but not in thapsigargin supplemented ($H = 20.89$, $p = 0.000$. Pairwise comparisons Normal-Thapsigargin: $U = 23.6$, $p = 0.000$; Ca2+ free – Thapsigargin: $U = 31.39$, $p = 0.000$). Error bars are standard error of the mean.

Figure 5: **Changes in gene expression following different LI-rMS stimulation protocols.** A: Heat map showing changes in expression (log_2 fold change) of the 16 genes that were significantly (asterisks) regulated following LI-rMS stimulation at one or more frequencies. B: Venn diagram showing number of changes in gene expression that are common to all frequencies and those that are specific to individual frequencies. C: Biofunctions of the 16 modulated genes as identified in Ingenuity Pathway analysis.

Figure 6: Representations of the relationships between 15 genes that were significantly regulated following LI-rMS stimulation. A. Pathway diagram obtained from Ingenuity Pathway Analysis showing the relationship between the genes examined following LI-rMS (blue = 1 Hz; green = 10 Hz and red = BHFS). Dark shading indicates upregulation and light

shading indicates downregulation. B. Regulated genes (in ovals) are situated within the cell survival and cell death pathways (see also Table 2 and Fig 5C). Non-regulated genes are included to provide context.

Figure
Click here to download high resolution image

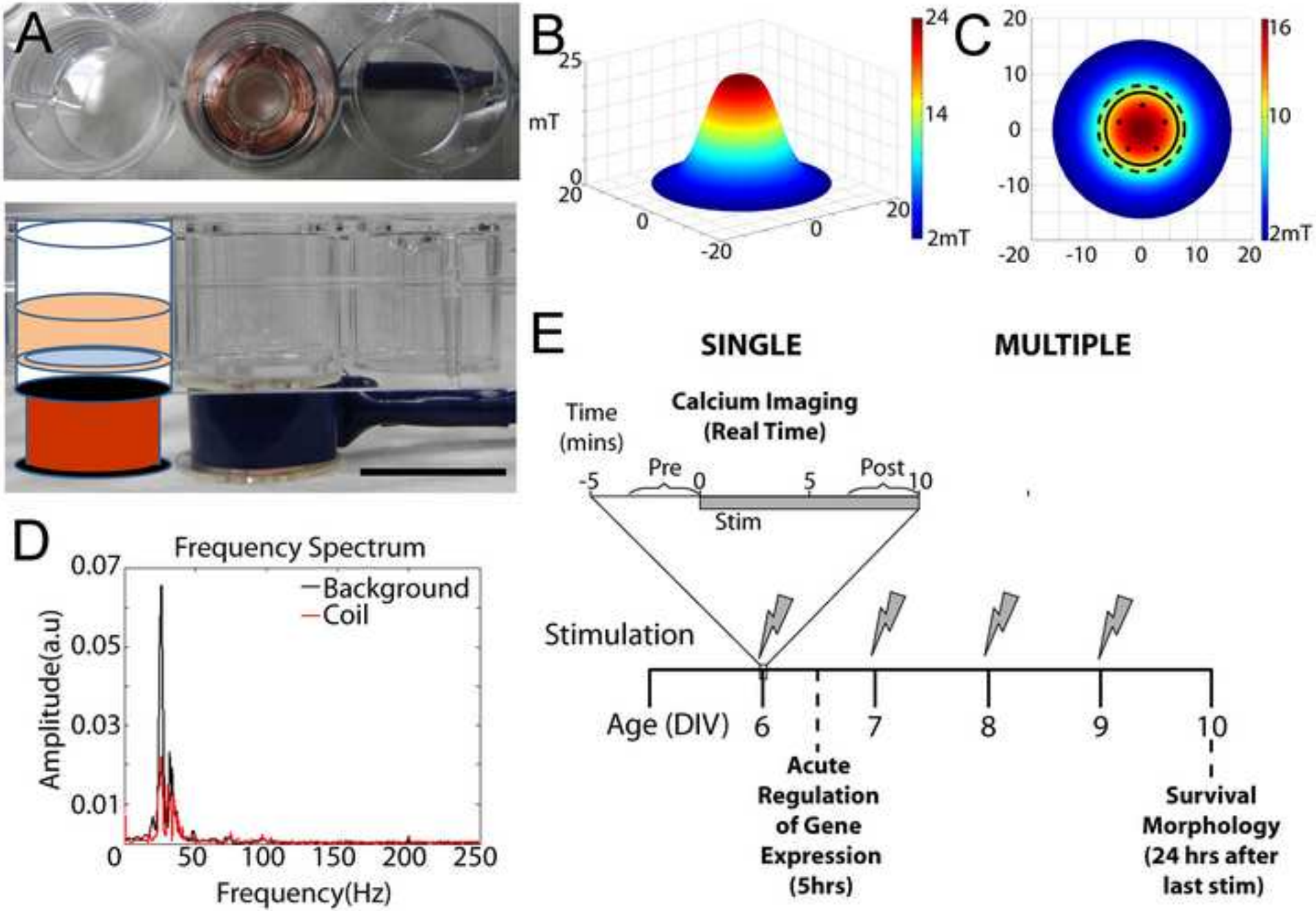

Figure
Click here to download high resolution image

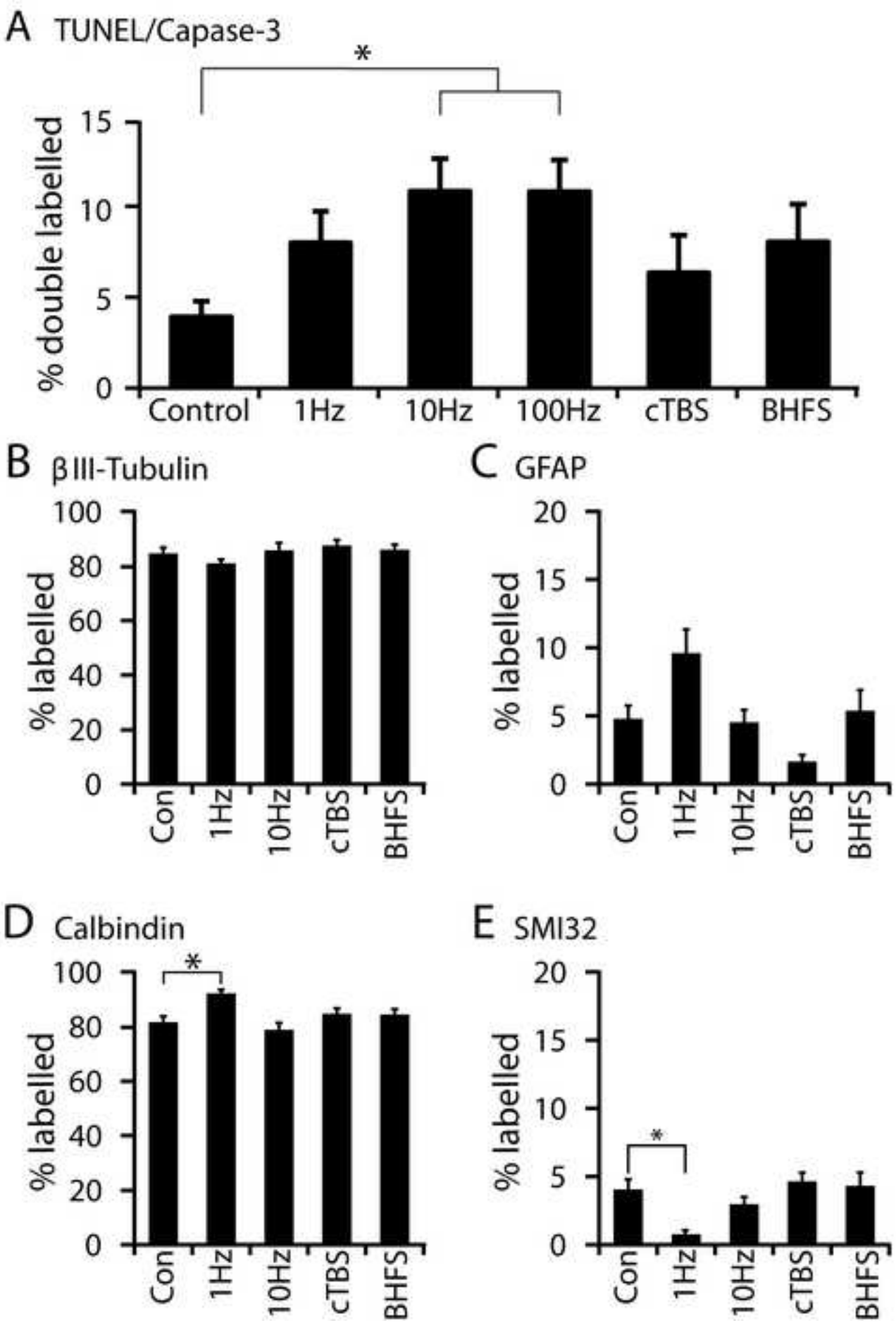

Figure

Click here to download high resolution image

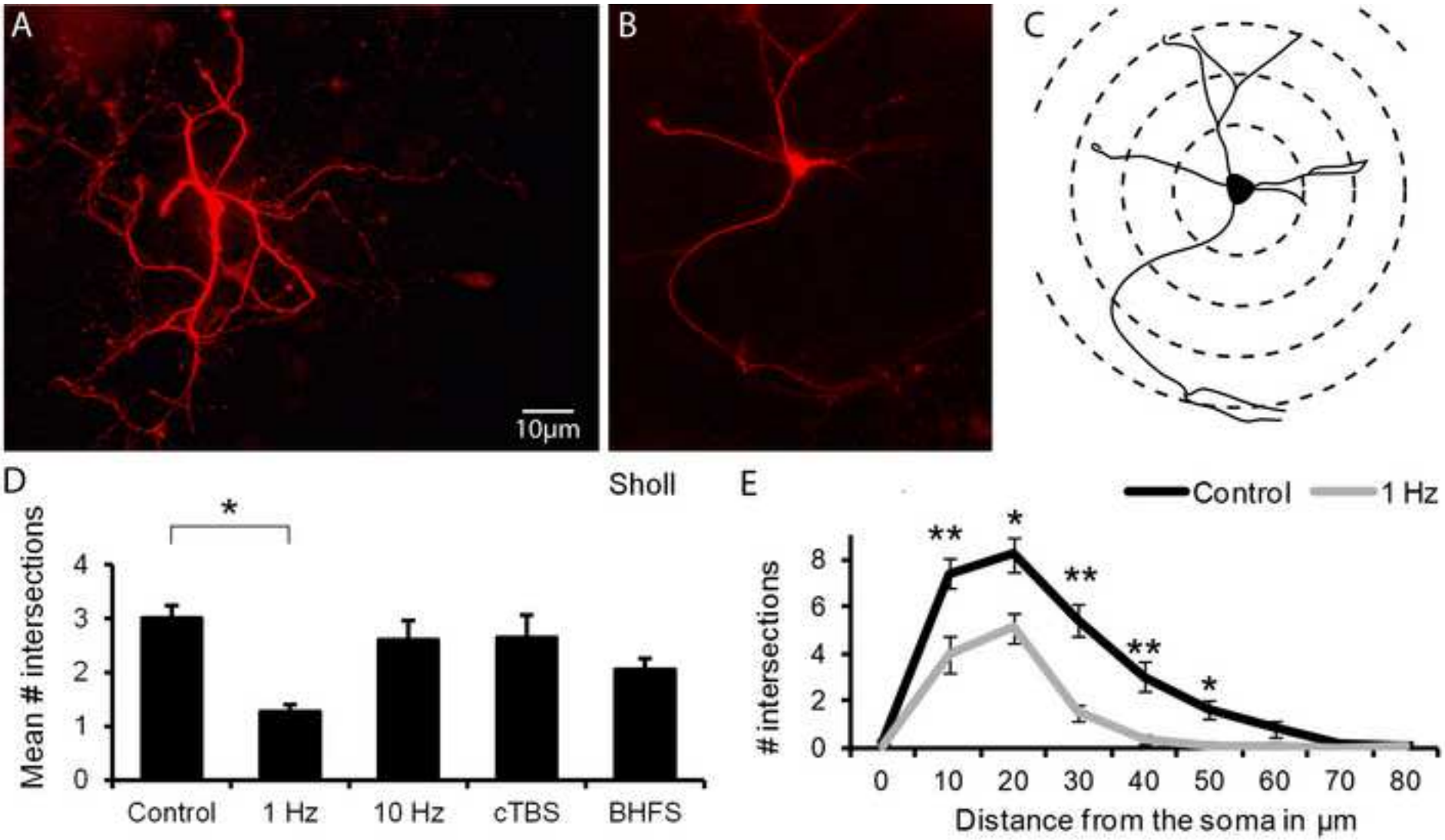

Figure
Click here to download high resolution image

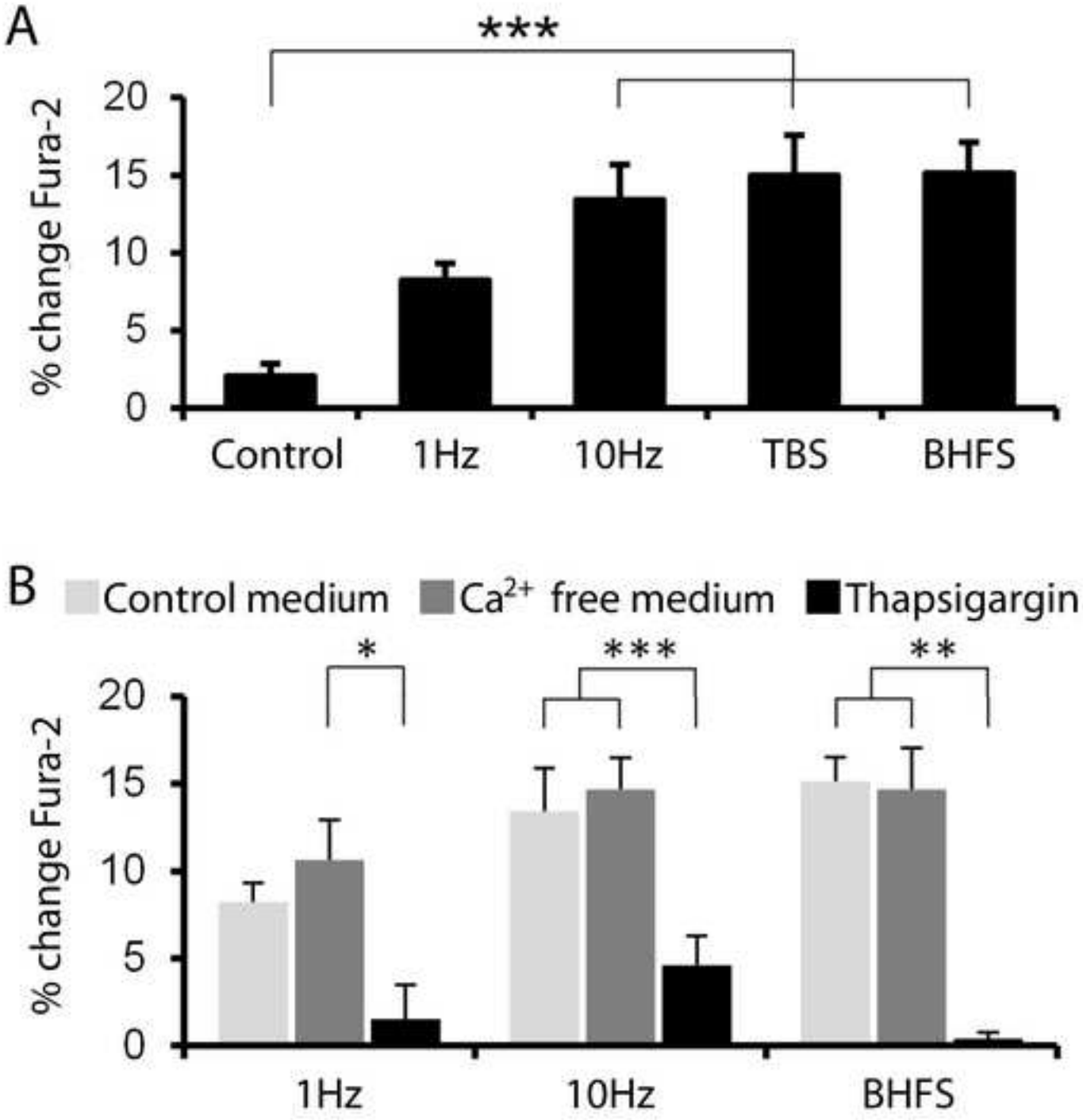

Figure
Click here to download high resolution image

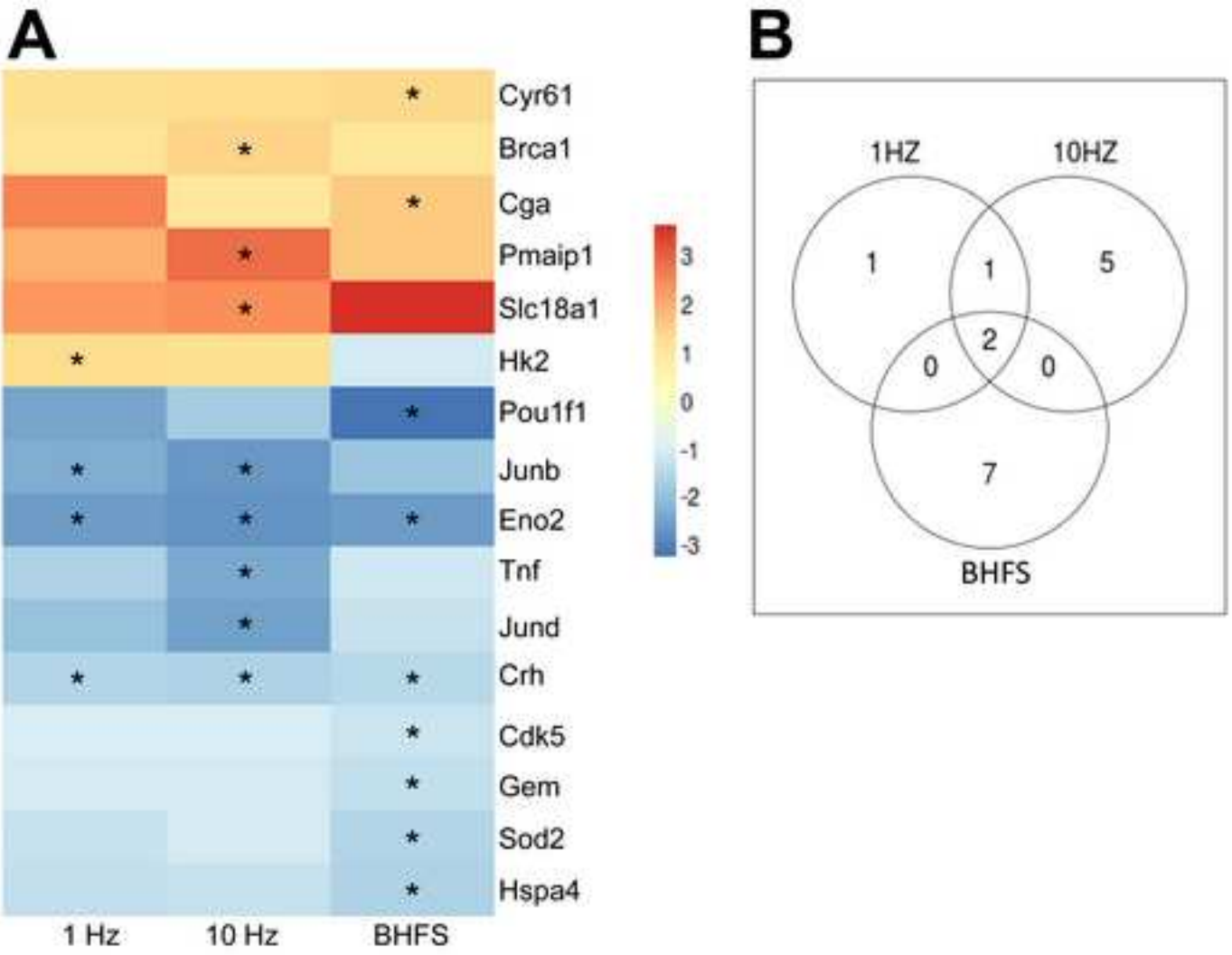

C

Molecules in Network	Focus Molecules	Top Functions
Brca1, Cdk5, Cga, Crh, Cyr61, Eno2, Gem, Hk2, Hspa4, Junb, Jund, Pmaip1, Pou1f1, Slc18a1, Sod2, Tnf, TSHB, GH2, Crhr	15	Cell Death and Survival, Cell Cycle, Cellular Development, Endocrine System Disorders, Cellular Growth and Proliferation, Hematological System Development and Function
Slc18	1	Cell-To-Cell Signaling and Interaction, Nervous System Development and Function, Cellular Growth and Proliferation

Figure

Click here to download high resolution image

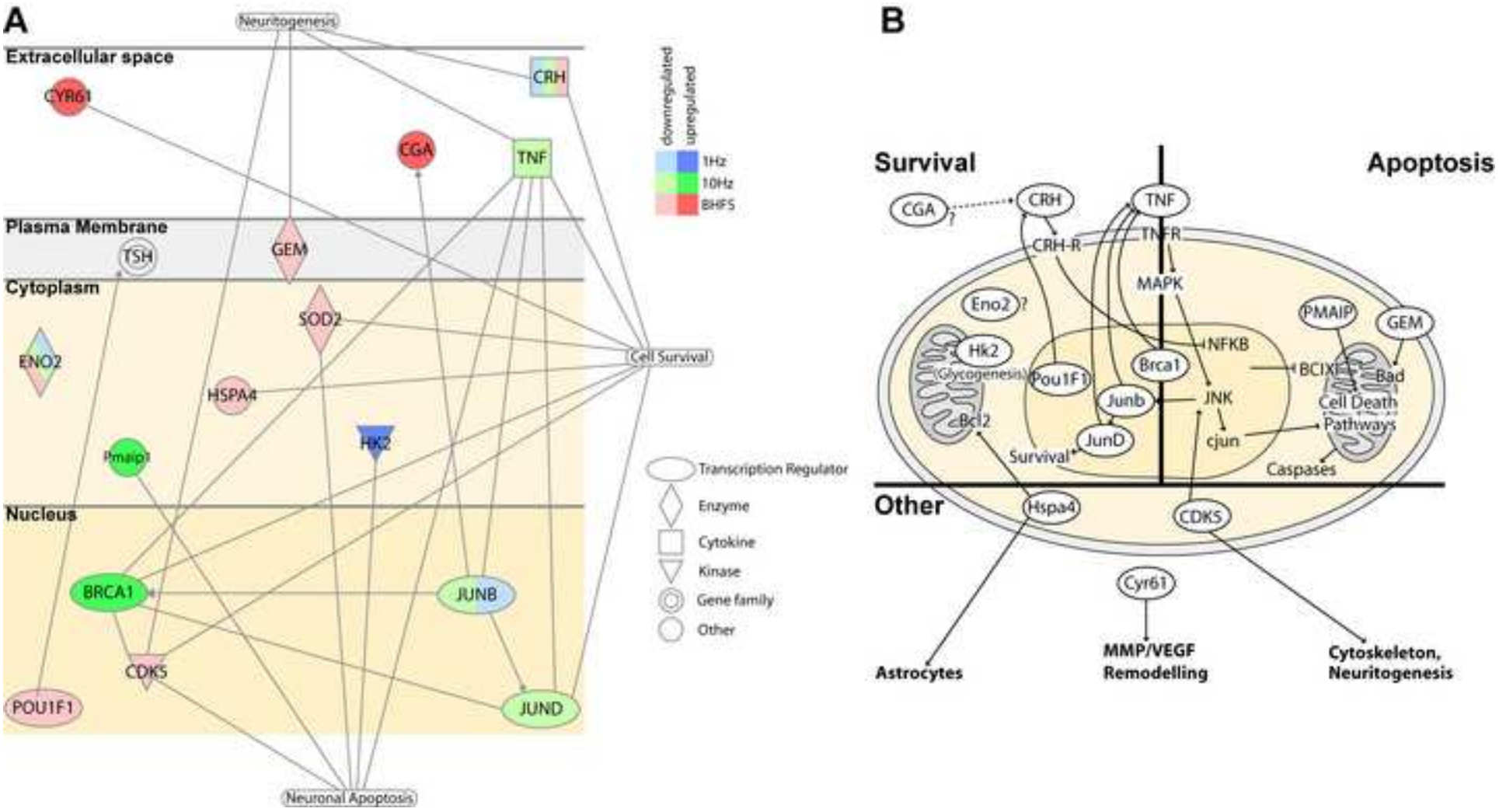

Table

Table 1: Total number of pulses delivered during 10 minutes for each frequency

Frequency	**Total pulses delivered in 10 minutes**
1 Hz	600
10Hz	6,000
100 Hz	60,000
cTBS	7,000
BHFS	120,000

Table

Table 2: List of genes that were significantly up or down regulated (Student t-test) five hours after a single PMF stimulation at 1Hz, 10Hz or BHFS frequencies. Fold change (primary colours indicate up-regulation and pastels indicate down-regulation) and p-values are relative to unstimulated controls.

ID	Entrez Gene Name	1Hz p-value	1 Hz Log FC	10 Hz p-value	10Hz Log FC	BHFS p-value	BHFS Log FC	Function	Type(s)
Brca1	breast cancer 1, early onset	0.27	1.200	**0.03**	**1.530**	0.62	1.070	Cell survival	transcription regulator
Cdk5	cyclin-dependent kinase 5	0.75	-1.030	0.68	-1.040	**0.03**	**-1.220**	Cytoskeletal remodelling	Nuclear kinase
Cga	glycoprotein hormones, alpha polypeptide	0.20	2.620	0.75	1.050	**0.04**	**1.640**	Cell survival	hormone
Crh	corticotropin releasing hormone	**0.01**	**-1.540**	**0.03**	**-1.620**	**0.003**	**-1.500**	Cell survival	Extracellular cytokine
Cyr61	cysteine-rich, angiogenic inducer, 61	0.19	1.290	0.06	1.370	**0.03**	**1.410**	Cytoskeletal remodelling	Extracellular protein
Eno2	enolase 2 (gamma, neuronal)	**0.04**	**-2.590**	**0.03**	**-2.740**	**0.03**	**-2.560**	Cell survival	Cytoplasmic enzyme
Gem	GTP binding protein overexpressed in skeletal muscle	0.85	-1.050	0.33	-1.110	**0.02**	**-1.330**	apoptosis	Membrane enzyme
Hk2	hexokinase 2	**0.04**	**1.360**	0.14	1.280	0.57	-1.090	Cell survival	Cytoplasmic kinase
Hspa4	heat shock 70kDa protein 4	0.09	-1.350	0.08	-1.280	**0.04**	**-1.610**		Cytoplasmic protein
Junb	jun B proto-oncogene	**0.04**	**-2.330**	**0.03**	**-2.670**	0.08	-1.860	Cell survival	transcription regulator
Jund	jun D proto-oncogene	0.07	-1.950	**0.007**	**-2.510**	0.33	-1.300	Cell survival	transcription regulator
Pmaip1	phorbol-12-myristate-13-acetate-induced protein 1	0.31	1.980	**0.03**	**2.860**	0.30	1.620	apoptosis	Cytoplasmic protein
Pou1f1	POU class 1 homeobox 1	0.26	-2.470	0.10	-1.760	**0.04**	**-3.220**	Cell survival	transcription regulator
Slc18a1	solute carrier family 18 (vesicular monoamine), member 1	0.37	2.320	**0.04**	**2.480**	0.23	3.650		Membrane transporter
Sod2	superoxide dismutase 2, mitochondrial	0.22	-1.310	0.71	-1.090	**0.03**	**-1.580**	apoptosis	Cytoplasmic enzyme
Tnf	tumor necrosis factor	0.34	-1.610	**0.04**	**-2.390**	0.89	-1.160	Cell survival	Extracellular cytokine

Supplementary Item

Click here to download Supplementary Item: Grehl et al supplementary 1.doc